

# Ratcheting behavior of pressurized corroded straight pipe subjected to cyclic bending

Xiaohui Chen<sup>1,2\*</sup>, Haofeng Chen<sup>3</sup>, Li Zhao<sup>1</sup>

<sup>1</sup>School of Control Engineering, Northeastern University, Qinhuangdao, 066004, China

<sup>2</sup>School of Mechanical Engineering & Automation, Yanshan University, Qinhuangdao, 066004, China

<sup>3</sup>Department of Mechanical & Aerospace Engineering, University of Strathclyde, G1 1XJ, UK

*\*Corresponding email: huixiao\_chen@126.com*

**Abstract:** The ratcheting behavior of pressurized corroded straight pipe subjected to cyclic bending is investigated using Chaboche model in the paper. The effects of defect length, depth and width and internal pressure on ratcheting strain are studied. The results show that the ratcheting strain increases with the increase of defect length  $L/D$ , depth  $H/T$ , circumferential length and internal pressure. Moreover, in order to analyze the effect of defect size on ratcheting strain of corroded straight pipe, calculation schemas are established according to orthogonal design method (ODM). Finally, dimensionless relations of both circumferential and longitudinal ratcheting strains to defect length, depth, width and internal pressure are established based on the multiple regression method.

**Keywords:** Corroded straight pipe, Chaboche model, Ratcheting strain, Orthogonal design method, Multiple regression method

## 1. Introduction

Chemical composition of 316 stainless steel includes Mo element which increases substantially its heat resistance and corrosion resistance. Thus, 316 stainless steels are widely used in heat exchange equipment, transportation pipelines of crude oil, nature gas pipelines, and so on where most pipes run under high temperature environment. The pipes are not only subjected to internal pressure, but also subjected to bending loading due to thermal expansion and shocks induced from sudden opening and closing of relief valves. In addition, these pipes are under cyclic mechanical and/or thermal loading, which would result in cyclic plastic strain accumulation, namely ratcheting effect. Ratcheting deformation results in decrease of fatigue life of pipes or malfunction due to excessive deformation. Therefore, during the design of pressurized piping, especially in power plant industries, ratcheting and ratcheting fatigue must be taken into consideration.

So far, ratcheting behaviors of pipes have been studied in two directions. On the one hand, ratcheting experiments are carried out for straight pipes, elbows, branches and even piping systems. On the other hand, ratcheting behaviors of pipe are simulated based on the Armstrong-Frederick type nonlinear kinematic hardening rule such as Bilinear [1], Multilinear [2], Armstrong and Frederic [3], Chaboche [4,5], modified Chaboche [6,7], Ohno-Wang [8,9], modified Ohno-Wang (10-15), Abdel Karim-Ohno[16] and modified Abdel Karim-Ohno[17,18], etc.

In 2013, Chen et al. [19] summarized experimental and numerical studies on piping components (such as straight pipes, elbows, branch and piping system) with mechanical ratcheting and thermal ratcheting, shakedown, fatigue failure responses. For elbow pipe subjected to internal pressure and bending loading, the maximum ratcheting strain occurred mainly in the hoop direction of flanks. Hoop ratcheting strain at intrados was found for individual elbow specimen. For pressurized straight pipe

under cyclic bending loading, the maximum ratcheting strain occurred mainly in the hoop direction of the center of straight pipe. For straight pipe and elbow pipe, the initial rate of ratcheting strain was large and then it decreased in the subsequent cycles. Ratcheting strain rate increased with the increase of bending loading level at a constant internal pressure. Moreover, it indicated that ratcheting strain of piping components had not been predicted well even by the advanced constitutive models. Thus, it was essential to critically evaluate the widely used and recently developed constitutive models against their simulation capability of component responses for determining the state-of-the-art constitutive modeling features and future model development needs. Ratcheting strains of pressurized piping components such as elbow pipe and straight pipe with or without local wall thinning under cyclic loading, have been also studied by experiments and finite element analysis after 2013 [20-36].

The orthogonal design method is widely used in many fields, but has not been induced for estimating ratcheting strain of materials/structures. In this paper, it is employed to optimize roughly calculated ratcheting strain of pipe. This method has been used in both theoretical and application ways [38, 39]. The ODM samples a small number of evenly distributed points over a large search space. Then it statistically summarizes a prospective good solution. The application of this method is much wider, for example, chemical and biological fields, image process, laser polishing, software testing technique, algorithm, semiconductor manufacturing, optics and robust design. Based on limit load analysis, Tan et al. [40] studied the chamber structure of rectangular vessels by means of nonlinear finite element analysis. With the help of the orthogonal design method, the influences of rib thickness, height and shell thickness on limit load were indicated. Sun et al. [41] used orthogonal design method to determine ratcheting boundary of pressurized lateral nozzle to cylinder with various dimensions. The empirical equations were obtained which would be helpful for anti-ratcheting design.

The engineering pipes operating in acid and alkali environments for a long time are vulnerable to corrosion. Once the pipes subjected to internal pressure and cyclic loading are corroded, damage behavior is easily to emerge, which imposes higher risk and failure probability during practical operation. Therefore, ratcheting behavior of straight pipe with local wall thinning under steady internal pressure and in-plane bending is investigated by using Chaboche model in the paper. The effect of internal pressure, defect axial, circumferential length and depth on ratcheting behavior of straight pipe is studied. Finally, the orthogonal design method and multiple regression method are used, where dimensionless relations of circumferential and longitudinal ratcheting strain are obtained.

## 2. Constitutive model

The software ABAQUS [42] employs the combination of nonlinear isotropic hardening and Chaboche kinematic hardening rule which is used to predict mechanical behaviours of component under cyclic loading. Nonlinear kinematic hardening model in ABAQUS must follow yield surface equation, flow rule and kinematic hardening rules.

(1) Yield surface equation:

$$F = f(\boldsymbol{\sigma} - \boldsymbol{\alpha}) - \sigma^0 = 0 \quad (1)$$

where  $\sigma^0$  is yield stress,  $f(\boldsymbol{\sigma} - \boldsymbol{\alpha})$  is equivalent Mises stress:

$$f(\boldsymbol{\sigma} - \boldsymbol{\alpha}) = \sqrt{\frac{3}{2}(\boldsymbol{S} - \boldsymbol{\alpha}^{dev}) : (\boldsymbol{S} - \boldsymbol{\alpha}^{dev})} \quad (2)$$

where  $\boldsymbol{S}$  is deviatoric stress tensor,  $\boldsymbol{\alpha}^{dev}$  is a part of deviatoric backstress tensor:

(2) Plastic flow rate

$$\dot{\boldsymbol{\varepsilon}}^{pl} = \frac{\partial F}{\partial \boldsymbol{\sigma}} \dot{p} \quad (3)$$

where  $\dot{\boldsymbol{\varepsilon}}^{pl}$  represents the rate of plastic flow and  $\dot{p}$  is the equivalent plastic strain rate which is

expressed as follows:

$$\dot{p} = \sqrt{\frac{2}{3} \dot{\boldsymbol{\varepsilon}}^{pl} : \dot{\boldsymbol{\varepsilon}}^{pl}} \quad (4)$$

### (3) Kinematic hardening rule

Each backstress should satisfy the following kinematic hardening rule without considering the influence of temperature and field variables.

$$\boldsymbol{\alpha} = \sum_{k=1}^N \boldsymbol{\alpha}_k \quad (5)$$

$$d\boldsymbol{\alpha}_k = \frac{2}{3} C_k d\boldsymbol{\varepsilon}^{pl} - \gamma_k \boldsymbol{\alpha}_k dp \quad (6)$$

where  $N$  represents the number of backstress components, the parameters  $C_k$  and  $\gamma_k$  are material parameters which are determined by cyclic strain test of materials.

### (4) Isotropic hardening rule

Isotropic hardening rule which is the function of equivalent plastic strain is used to define the evolution of shape of yield surface. Isotropic hardening rule is expressed as follows:

$$\sigma^0 = \sigma_{in} + Q_{\infty} \left( 1 - e^{-b\bar{\varepsilon}^{pl}} \right) \quad (7)$$

where  $\sigma_{in}$  denotes initial yield stress.  $Q_{\infty}$  and  $b$  are material parameters, i.e.  $Q_{\infty}$  is the maximum value of yield surface size,  $b$  is the rate of yield surface size with changing plastic strain.

The materials investigated in this paper is 316 stainless steel whose chemical composition is shown in

Table 1 and mechanical properties are listed in Table 2. The materials parameters [43] are as follows:  $E = 192\text{GPa}$  ,  $\nu = 0.3$  ,  $\sigma_0 = 120\text{MPa}$  ,  $C_1 = 2.067\text{GPa}$  ,  $\gamma_1 = 44.7$  ,  $C_2 = 246.2\text{GPa}$  ,  $\gamma_2 = 2551.4$  ,  $Q_\infty = 120\text{MPa}$ , and  $b = 13.2$ . Half-cycle method in ABAQUS is used to determine kinematic hardening parameters of 316 stainless steel.

Table 1 Chemical composition of 316 stainless steel (% in weight)

Material	C	Si	Mn	P	S	Ni	Cr	Mo	Co	Fe
316	≤0.08	≤1	≤2	≤0.045	≤0.030	10.0~14.0	16.0~18.0	2.00-3.00		
	0.018	0.35	1.62	0.024	0.002	11.08	16.7	2.13	0.2	Balance

Table 2 Mechanical properties of 316 stainless steel

Material	Elastic modulus	Poisson's	Initial yield	Yield strength	ultimate strength	HBS	HRB	HV
	E/GPa	ratio $\nu$	stress /MPa	$\sigma_{0.2}$ /MPa	$\sigma_b$ /MPa			
316	192	0.3	120	≥205	≥520	≤187	≤90	≤200

### 3. Ratcheting effect of pressurized corroded pipes under in-plane reversed bending

#### 3.1 Geometric model

Cosham et al. [44] indicated that, as general pipeline was thin-shell structure, no much difference exists between inside and outside wall thickness of corroded pipe. Therefore, this study assumes that outside wall thickness of pipe is reduced, as given in Fig. 1. In fact, the shape of pipe corrosion defects is very complicated and is difficult to be described using geometric model. Therefore, it must be simplified before finite element model building. In ANSI/ASME code, corrosion defects of pipes are usually idealized into semi-elliptic [45,46]. Thus, in this study, the shape of corrosion defects of pipes is taken as semi-elliptic, as given in Fig. 1.

Fig. 1 shows the geometric diagram of pressurized corroded pipes under in-plane bending loading. The geometric shape of longitudinal corrosion defect is elliptical. The two defects are located at the top and bottom surface of pipe center. The straight pipe is divided into ten segments along the longitudinal direction, including nine points, namely 1A, 2A, 2B, 3A, 3B, 4A, 4B, 5A, 5B, as shown in Fig. 1.

Four-point bending test scheme is adopted in this study. The points 3A and 3B correspond to the loading positions of four-point bending. The points 5A and 5B are two supporting positions. In the four-point bending experiment, the corroded pipes are subjected to internal pressure and in-plane reversed bending.

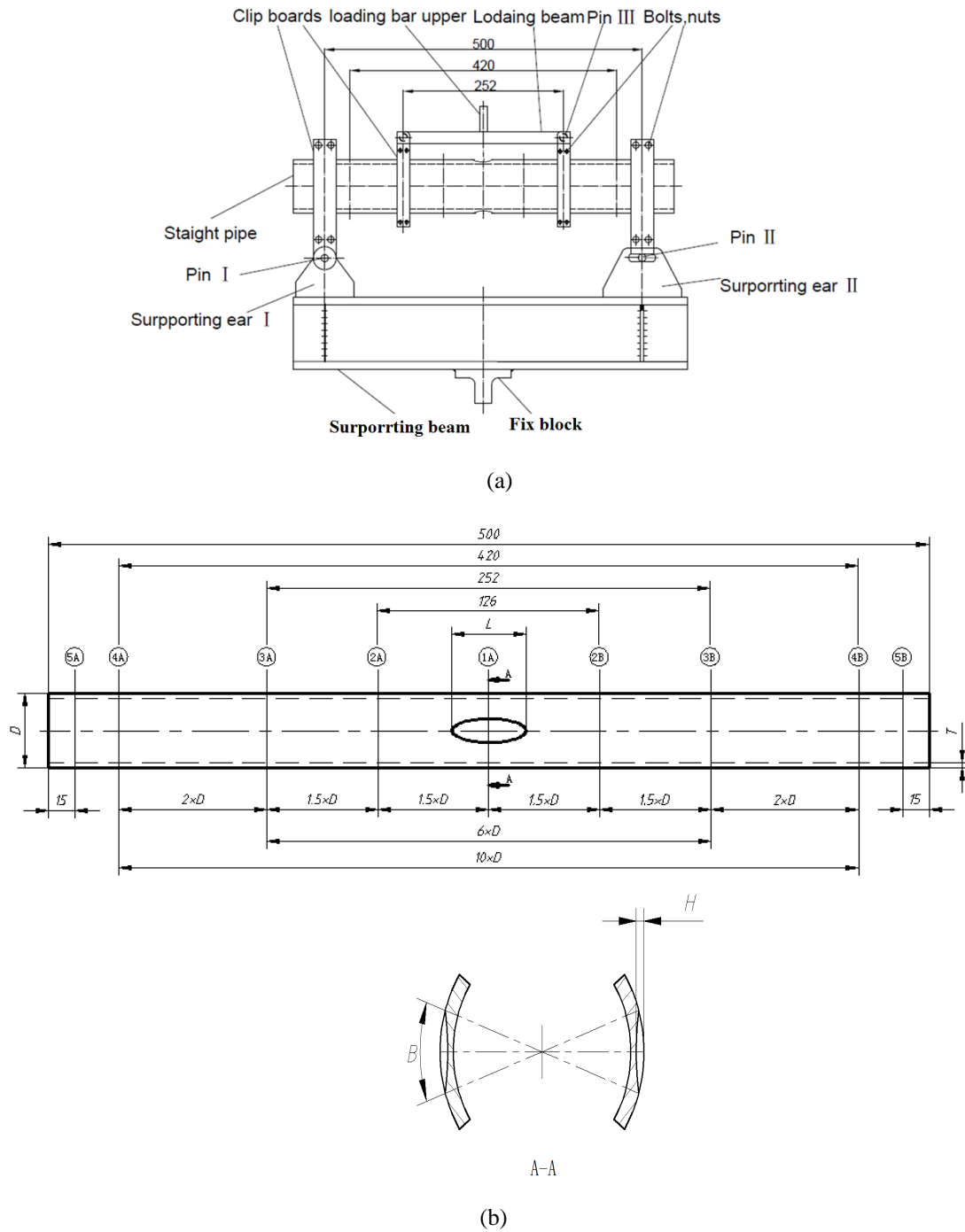


Fig. 1 The specimen of pressurized corroded pipe

### 3.2 Finite element model

According to geometric structure, boundary conditions and loadings, a quarter of finite element model is established using a quadratic three-dimensional solid element C3D20 with twenty nodes and twenty-seven integration points, as given in Fig. 2. In order to reduce computing time and save resource, the defect meshes are developed with a denser mesh at the top and bottom of straight pipe, as shown in Fig. 2. Loading is applied in two steps. In the first step, internal pressure is applied to the internal surface. In the second step, internal pressure is kept constant and a cyclic moment is applied to a reference point (RP) connected to all existing nodes in the cross section of the model end. XoY plane is applied to the symmetric displacement constraints. The displacement constraints was applied in the y-direction and z-direction at reference point (RP). The rotation constraints was applied in the x-direction and z-direction at reference point (RP).

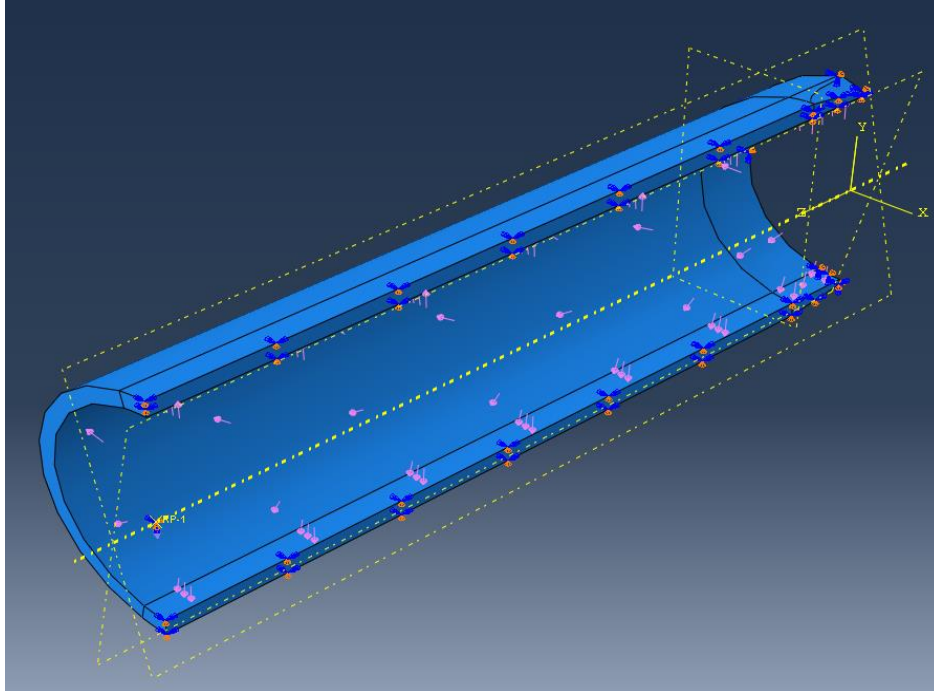


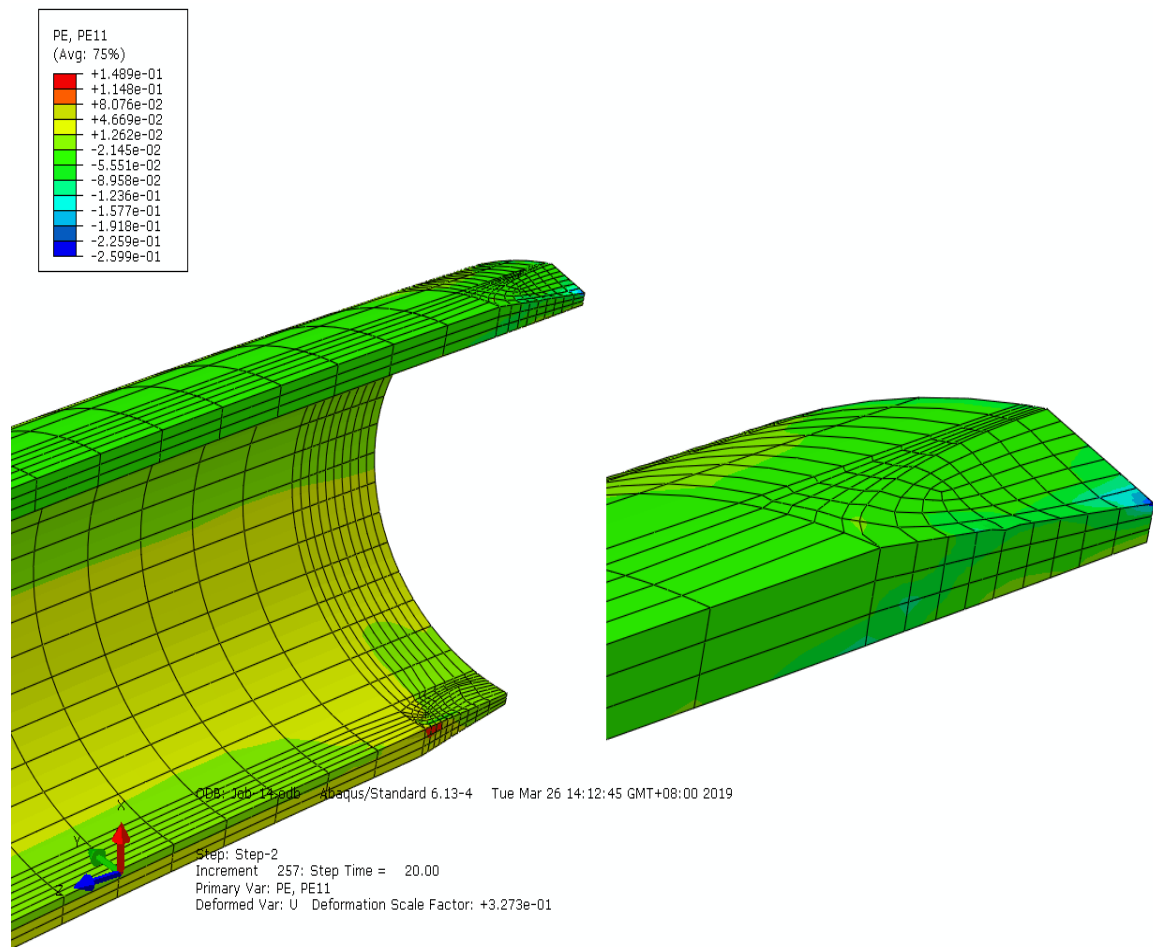
Fig. 2 Boundary conditions of straight pipes

In this study, ratcheting strain  $\varepsilon_r$  is determined in the following.

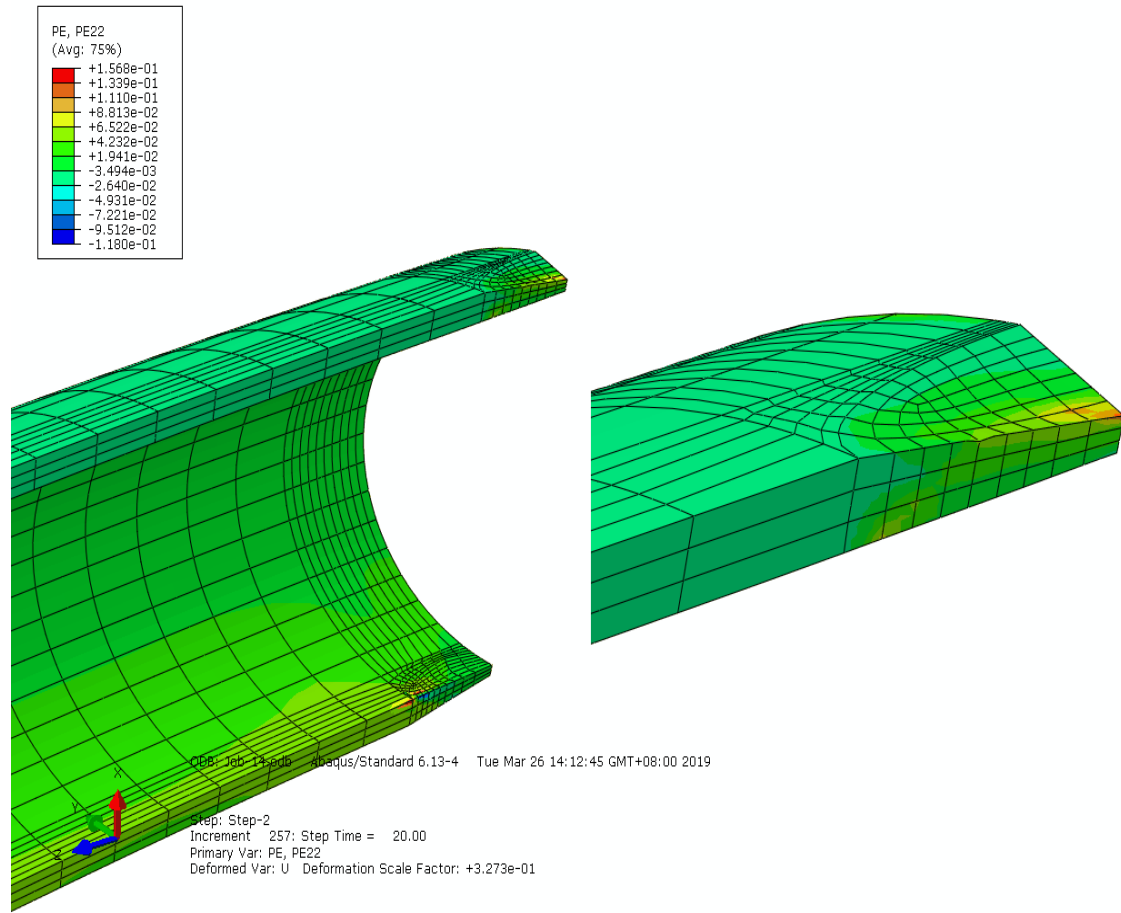
$$\varepsilon_r = \frac{1}{2}(\varepsilon_{\max} + \varepsilon_{\min}) \quad (8)$$

where  $\varepsilon_{\max}$  and  $\varepsilon_{\min}$  were the maximum strain and minimum strain in each cycle, respectively.

Fig. 3 shows the contour of circumferential and axial ratcheting strain for corroded straight pipe subjected to internal pressure of 12 MPa and cycling bending of  $2\pm 5$  kN, respectively. The relationship between circumferential, longitudinal plastic strain and stress is shown in Fig. 4. It indicated that there is a dip in Fig. 4 (a) at small plastic strain, which is attributed to strain and stress value of “unique nodal A” of the element in ABAQUS, as given in Fig. 4(b). The node and integration point in finite element method are different. Integration point is Gauss point. The stress of a node is determined by means of the stress inset or extension of several integration points.



(a) Hoop plastic strain



(b) Axial plastic strain

Fig. 3 Plastic strain contour

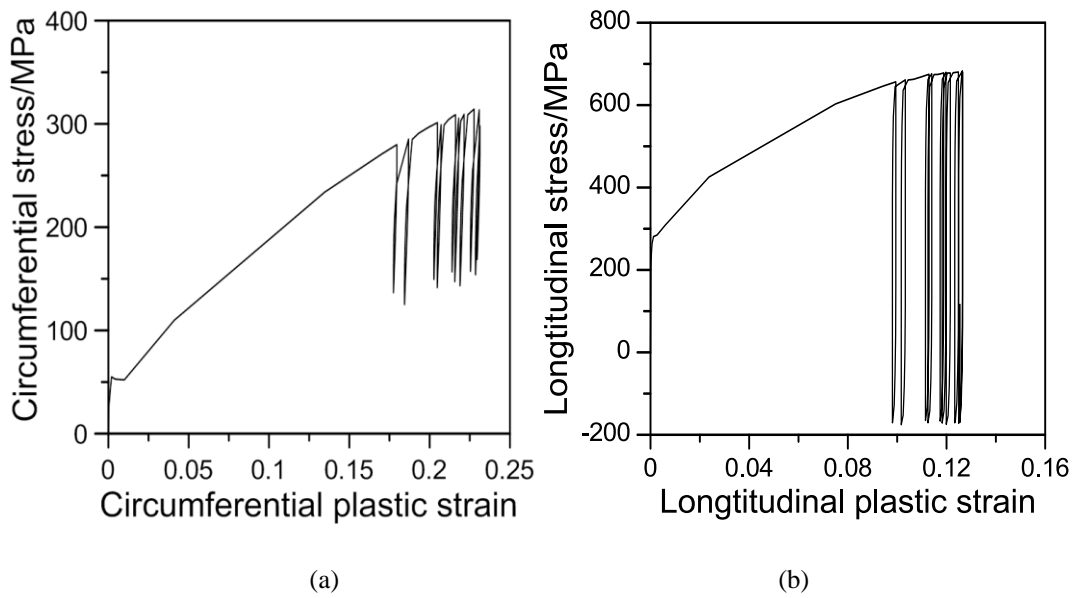


Fig. 4 The relationship of circumferential and longitudinal plastic strain and stress

Fig. 5 gives the relationship of time and circumferential and longitudinal plastic strain. It is found in Fig. 5 that the circumferential and longitudinal plastic strain increase with the increasing of time. The circumferential plastic strain is larger than the longitudinal plastic strain.

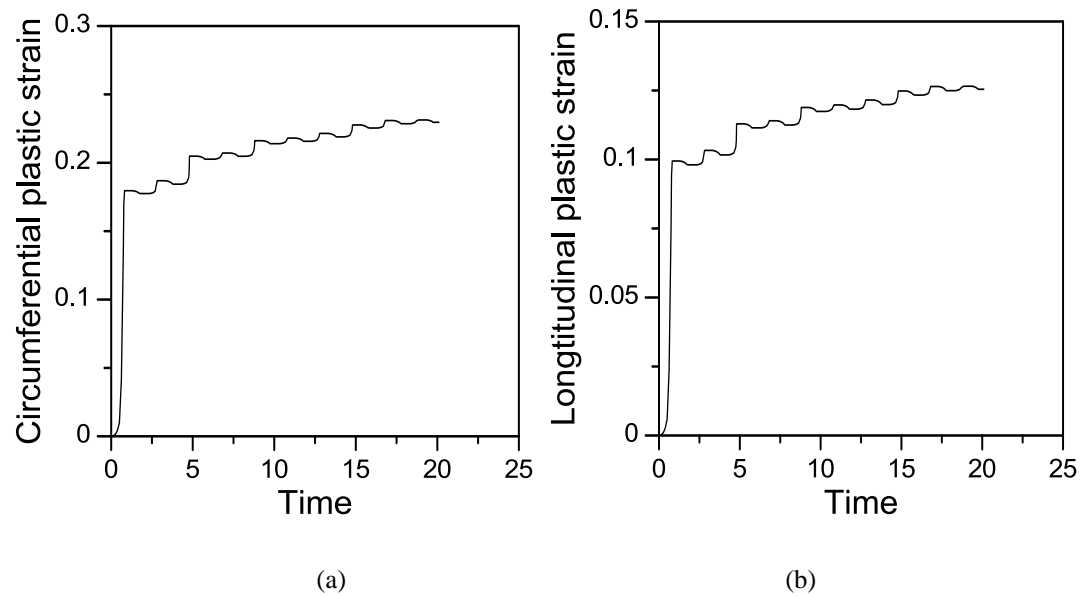


Fig. 5 The relationship of time and circumferential and longitudinal plastic strain

### 3.3 Analysis and Discussion

According to ASME code, when the corroded maximum depth is less than 20% of the wall thickness of pipes, the corroded pipes can be still used. When the corroded maximum depth is more than 80% of the wall thickness, the corroded pipes must be replaced or repaired [47]. In practical engineering, the defect depth is generally less than 70% of the wall thickness [48]. In conclusion, the defect deep  $H/T$  is 0.5, 0.6 and 0.7 in this study.

Cosham et al. [44] concluded that when the pipes were subjected to bending load, the effect of defect circumferential length on limit load was very large. In order to simplify model and obtain accurate results, the defect circumferential angle  $B$  is arbitrary selected, namely  $B=24^\circ$ ,  $32^\circ$  and  $40^\circ$ . For defect axial length of pipes, bending load did not affect plastic failure. But the effect of axial length of

defect on the ratcheting strain of pipe is investigated in this study, where the axial length  $L$  of defect is selected as 21mm, 29.4mm and 42mm, respectively.

The effects of defect size, internal pressure and cyclic bending on ratcheting behavior of 316 austenitic stainless steel straight pipe are studied. The outer diameter  $D$  of straight pipe is 42 mm, and wall thickness  $t$  is 2.7 mm. Cyclic in-plane bending is  $2\pm 5$ kN, and the number of cycles is ten. Defect length  $L=21$ mm, 29.4mm and 42mm, defect depth  $H=1.35$ mm, 1.62mm and 1.89mm, defect width  $B=24^\circ$ ,  $32^\circ$  and  $40^\circ$ . Internal pressure  $P=12$ MPa, 15MPa and 18MPa. Hoop ratcheting strain  $\varepsilon_{r\theta}$  and axial ratcheting strain  $\varepsilon_{rz}$  at position 1A of straight pipe at outside surface is studied in the following.

In order to comprehensively analyze the effect of defect geometry parameters on ratcheting behavior of straight pipe, the ODM is used to arrange schematic design. For calculating convenience, geometry parameters of defect sizes and straight pipe are expressed as dimensionless forms, namely  $L/D$ ,  $H/T$ ,  $B/90^\circ$  and  $P/20$ . Orthogonal table  $L_9(3^4)$  is arranged in the study, where each factor has three “levels”, and hence there are 81 models, as listed in Table 3.

Table 4 gives all orthogonal analysis data.

Table 3 Experimental design with four factors and three levels per factor.

Levels \ Factors	$L/D$	$H/T$	$B/90^\circ$	$P/\sigma_{in}$
1	0.5	0.5	0.267	0.1
2	0.7	0.6	0.356	0.125
3	1	0.7	0.444	0.15

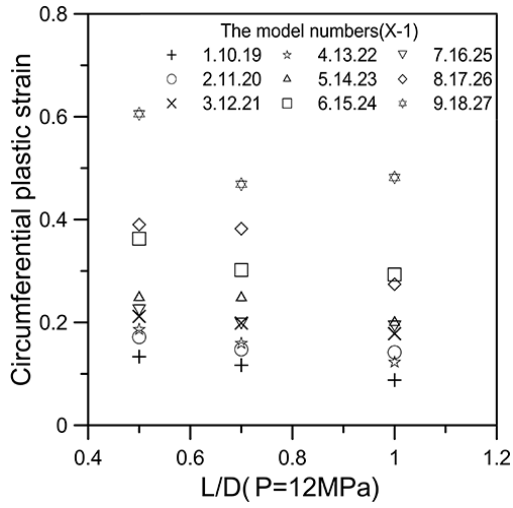
Table 4 Orthogonal analysis data

NO.	<i>L/D</i>	<i>H/T</i>	<i>B/90</i>	<i>P/σ<sub>in</sub></i>	NO.	<i>L/D</i>	<i>H/T</i>	<i>B/90</i>	<i>P/σ<sub>in</sub></i>
1-1	1(0.5)	1(0.5)	1(0.267)	1(0.1)	14-3	2(0.7)	2(0.6)	2(0.356)	3(0.15)
1-2	1(0.5)	1(0.5)	1(0.267)	2(0.125)	15-1	2(0.7)	2(0.6)	3(0.444)	1(0.1)
1-3	1(0.5)	1(0.5)	1(0.267)	3(0.15)	15-2	2(0.7)	2(0.6)	3(0.444)	2(0.125)
2-1	1(0.5)	1(0.5)	2(0.356)	1(0.1)	15-3	2(0.7)	2(0.6)	3(0.444)	3(0.15)
2-2	1(0.5)	1(0.5)	2(0.356)	2(0.125)	16-1	2(0.7)	3(0.7)	1(0.267)	1(0.1)
2-3	1(0.5)	1(0.5)	2(0.356)	3(0.15)	16-2	2(0.7)	3(0.7)	1(0.267)	2(0.125)
3-1	1(0.5)	1(0.5)	3(0.444)	1(0.1)	16-3	2(0.7)	3(0.7)	1(0.267)	3(0.15)
3-2	1(0.5)	1(0.5)	3(0.444)	2(0.125)	17-1	2(0.7)	3(0.7)	2(0.356)	1(0.1)
3-3	1(0.5)	1(0.5)	3(0.444)	3(0.15)	17-2	2(0.7)	3(0.7)	2(0.356)	2(0.125)
4-1	1(0.5)	2(0.6)	1(0.267)	1(0.1)	17-3	2(0.7)	3(0.7)	2(0.356)	3(0.15)
4-2	1(0.5)	2(0.6)	1(0.267)	2(0.125)	18-1	2(0.7)	3(0.7)	3(0.444)	1(0.1)
4-3	1(0.5)	2(0.6)	1(0.267)	3(0.15)	18-2	2(0.7)	3(0.7)	3(0.444)	2(0.125)
5-1	1(0.5)	2(0.6)	2(0.356)	1(0.1)	18-3	2(0.7)	3(0.7)	3(0.444)	3(0.15)
5-2	1(0.5)	2(0.6)	2(0.356)	2(0.125)	19-1	3(1)	1(0.5)	1(0.267)	1(0.1)
5-3	1(0.5)	2(0.6)	2(0.356)	3(0.15)	19-2	3(1)	1(0.5)	1(0.267)	2(0.125)
6-1	1(0.5)	2(0.6)	3(0.444)	1(0.1)	19-3	3(1)	1(0.5)	1(0.267)	3(0.15)
6-2	1(0.5)	2(0.6)	3(0.444)	2(0.125)	20-1	3(1)	1(0.5)	2(0.356)	1(0.1)
6-3	1(0.5)	2(0.6)	3(0.444)	3(0.15)	20-2	3(1)	1(0.5)	2(0.356)	2(0.125)
7-1	1(0.5)	3(0.7)	1(0.267)	1(0.1)	20-3	3(1)	1(0.5)	2(0.356)	3(0.15)
7-2	1(0.5)	3(0.7)	1(0.267)	2(0.125)	21-1	3(1)	1(0.5)	3(0.444)	1(0.1)
7-3	1(0.5)	3(0.7)	1(0.267)	3(0.15)	21-2	3(1)	1(0.5)	3(0.444)	2(0.125)
8-1	1(0.5)	3(0.7)	2(0.356)	1(0.1)	21-3	3(1)	1(0.5)	3(0.444)	3(0.15)
8-2	1(0.5)	3(0.7)	2(0.356)	2(0.125)	22-1	3(1)	2(0.6)	1(0.267)	1(0.1)
8-3	1(0.5)	3(0.7)	2(0.356)	3(0.15)	22-2	3(1)	2(0.6)	1(0.267)	2(0.125)

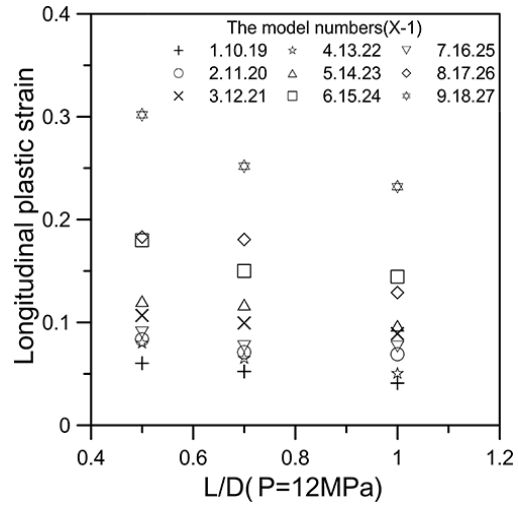
9-1	1(0.5)	3(0.7)	3(0.444)	1(0.1)	22-3	3(1)	2(0.6)	1(0.267)	3(0.15)
9-2	1(0.5)	3(0.7)	3(0.444)	2(0.125)	23-1	3(1)	2(0.6)	2(0.356)	1(0.1)
9-3	1(0.5)	3(0.7)	3(0.444)	3(0.15)	23-2	3(1)	2(0.6)	2(0.356)	2(0.125)
10-1	2(0.7)	1(0.5)	1(0.267)	1(0.1)	23-3	3(1)	2(0.6)	2(0.356)	3(0.15)
10-2	2(0.7)	1(0.5)	1(0.267)	2(0.125)	24-1	3(1)	2(0.6)	3(0.444)	1(0.1)
10-3	2(0.7)	1(0.5)	1(0.267)	3(0.15)	24-2	3(1)	2(0.6)	3(0.444)	2(0.125)
11-1	2(0.7)	1(0.5)	2(0.356)	1(0.1)	24-3	3(1)	2(0.6)	3(0.444)	3(0.15)
11-2	2(0.7)	1(0.5)	2(0.356)	2(0.125)	25-1	3(1)	3(0.7)	1(0.267)	1(0.1)
11-3	2(0.7)	1(0.5)	2(0.356)	3(0.15)	25-2	3(1)	3(0.7)	1(0.267)	2(0.125)
12-1	2(0.7)	1(0.5)	3(0.444)	1(0.1)	25-3	3(1)	3(0.7)	1(0.267)	3(0.15)
12-2	2(0.7)	1(0.5)	3(0.444)	2(0.125)	26-1	3(1)	3(0.7)	2(0.356)	1(0.1)
12-3	2(0.7)	1(0.5)	3(0.444)	3(0.15)	26-2	3(1)	3(0.7)	2(0.356)	2(0.125)
13-1	2(0.7)	2(0.6)	1(0.267)	1(0.1)	26-3	3(1)	3(0.7)	2(0.356)	3(0.15)
13-2	2(0.7)	2(0.6)	1(0.267)	2(0.125)	27-1	3(1)	3(0.7)	3(0.444)	1(0.1)
13-3	2(0.7)	2(0.6)	1(0.267)	3(0.15)	27-2	3(1)	3(0.7)	3(0.444)	2(0.125)
14-1	2(0.7)	2(0.6)	2(0.356)	1(0.1)	27-3	3(1)	3(0.7)	3(0.444)	3(0.15)
14-2	2(0.7)	2(0.6)	2(0.356)	2(0.125)					

### 3.3.1 The effect of defect axial length on ratcheting strain

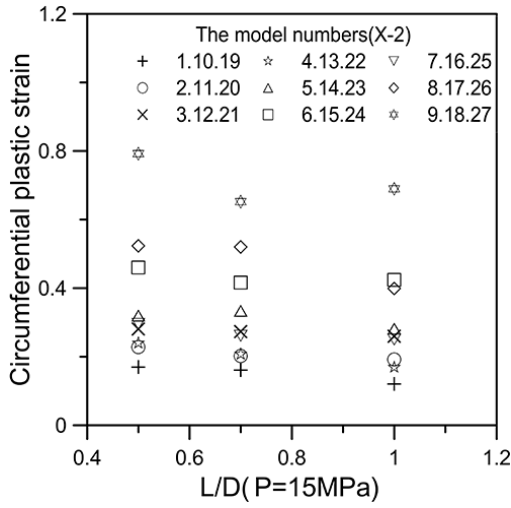
The effect of defect axial length  $L/D$  on ratcheting strain of straight pipe subjected to internal pressure ( $P=12\text{MPa}$ ,  $15\text{MPa}$  and  $18\text{MPa}$ , respectively) and cyclic bending is shown in Fig. 6. The relationship between hoop, axial ratcheting strain at position 1A and dimensionless defect axial length  $L/D$  is shown in Fig. 6, respectively. Fig. 7 shows the effect of different defect axial length such as 0.5, 0.7 and 1 on hoop and axial ratcheting behavior, respectively. It is found that the longer defect axial length  $L/D$ , the smaller the ratcheting strain.



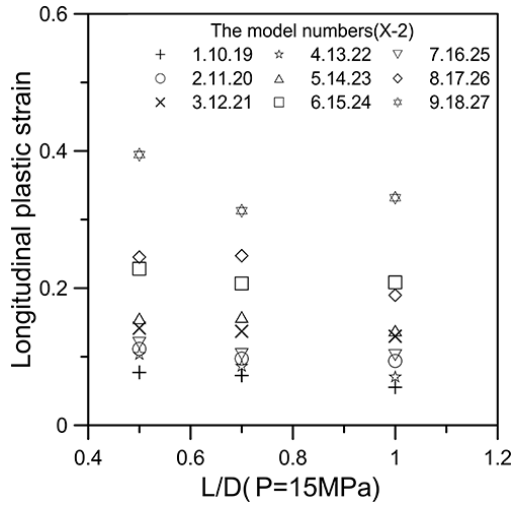
(a)



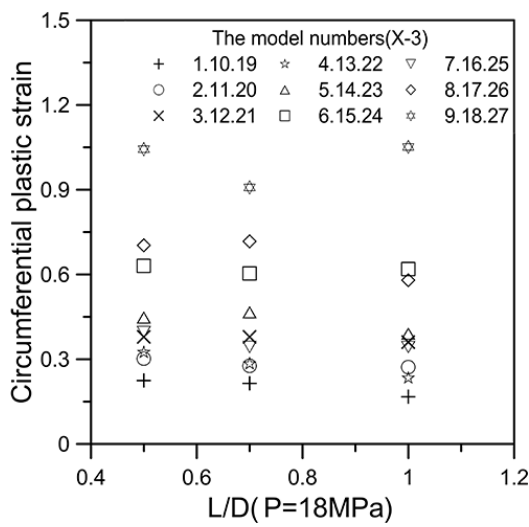
(b)



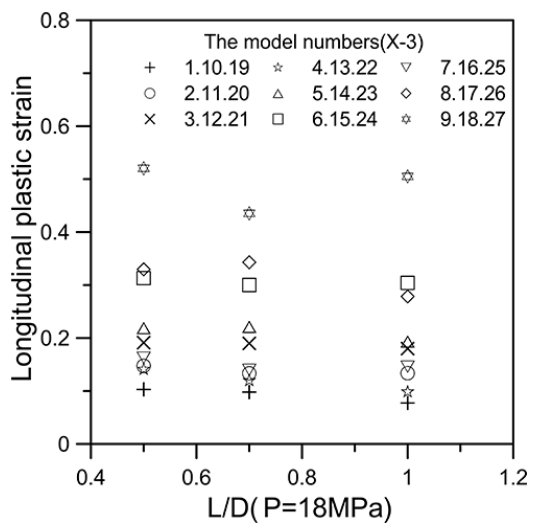
(c)



(d)



(e)



(f)

Fig. 6 The effect of defect axial length  $L/D$  on ratcheting strain under different internal pressure

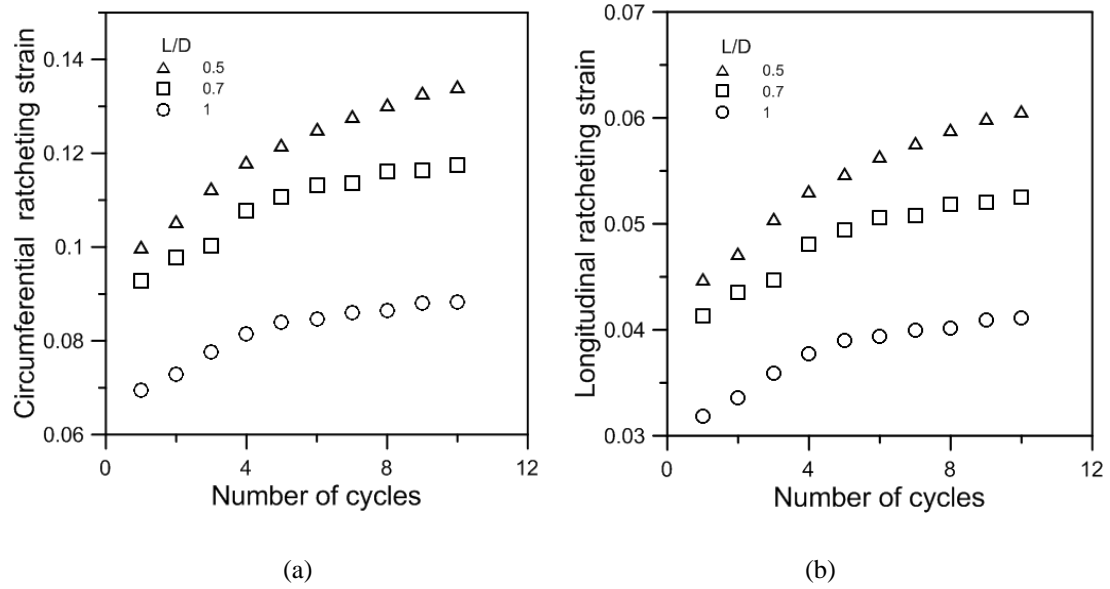
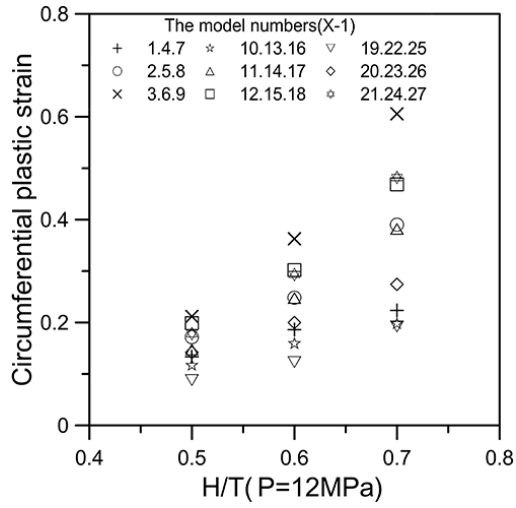


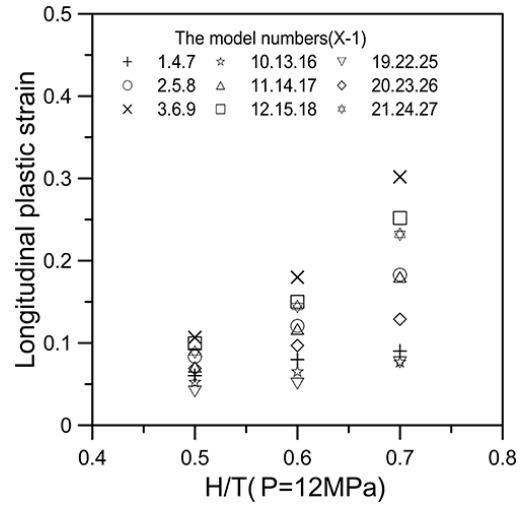
Fig. 7 Circumferential and longitudinal ratcheting strain versus number of cycles

### 3.3.2 The effect of defect depth on ratcheting strain

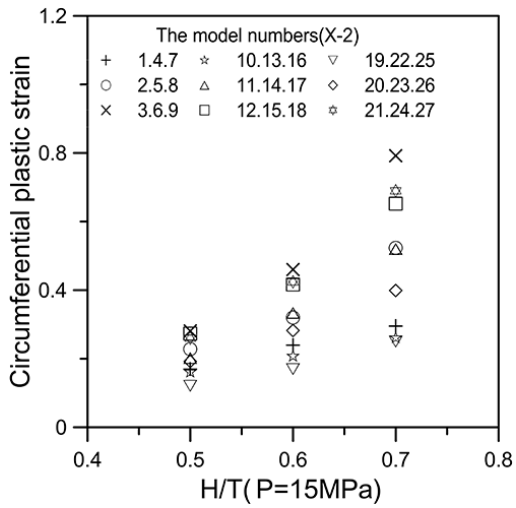
Fig. 8 shows the effect of defect depth  $H/T$  on ratcheting effect of straight pipe subjected to internal pressure ( $P=12\text{MPa}$ ,  $15\text{MPa}$  and  $18\text{MPa}$ , respectively) and cyclic bending. It shows the relationship between hoop, axial ratcheting strain at position 1A and dimensionless defect depth  $H/T$ . The effect of defect depth on ratcheting behavior is shown in Fig. 9. It is found that the ratcheting strain increases with the increase of defect depth  $H/T$ .



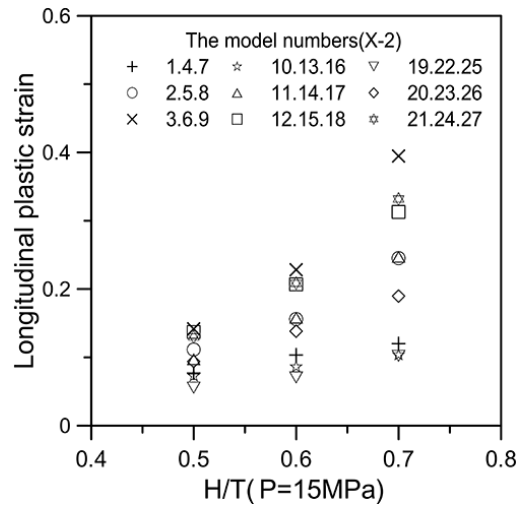
(a)



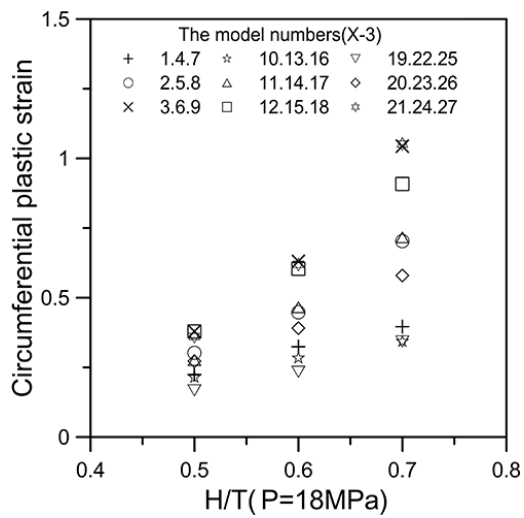
(b)



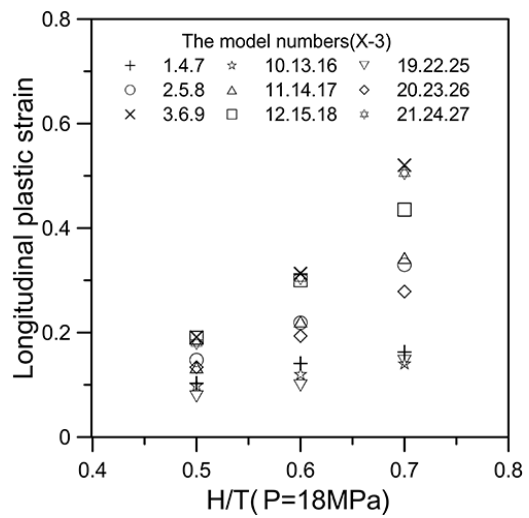
(c)



(d)



(e)



(f)

Fig. 8 The effect of defect depth  $H/T$  on ratcheting strain under different internal pressure

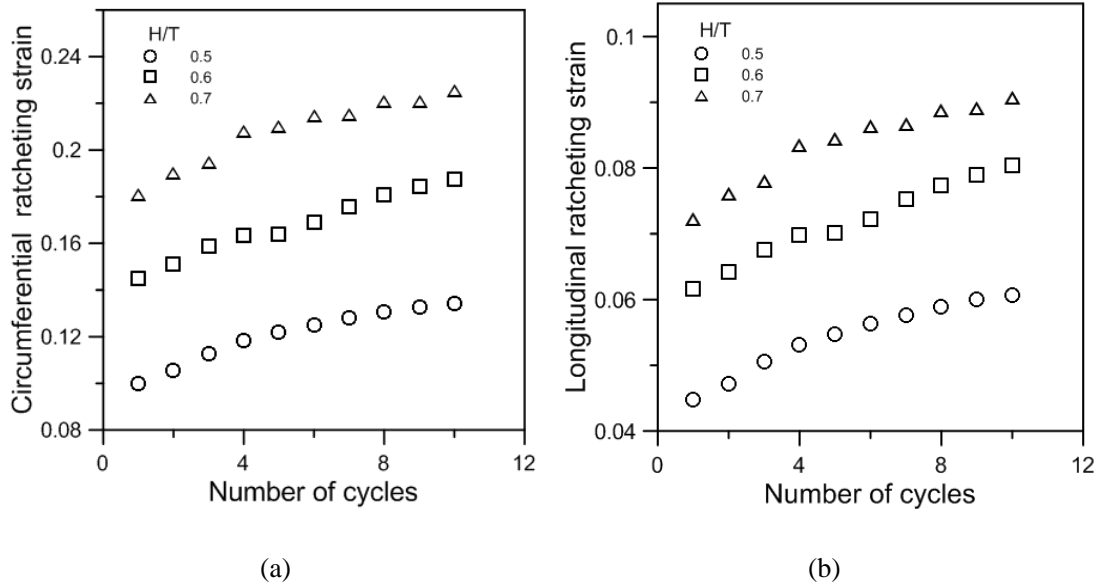
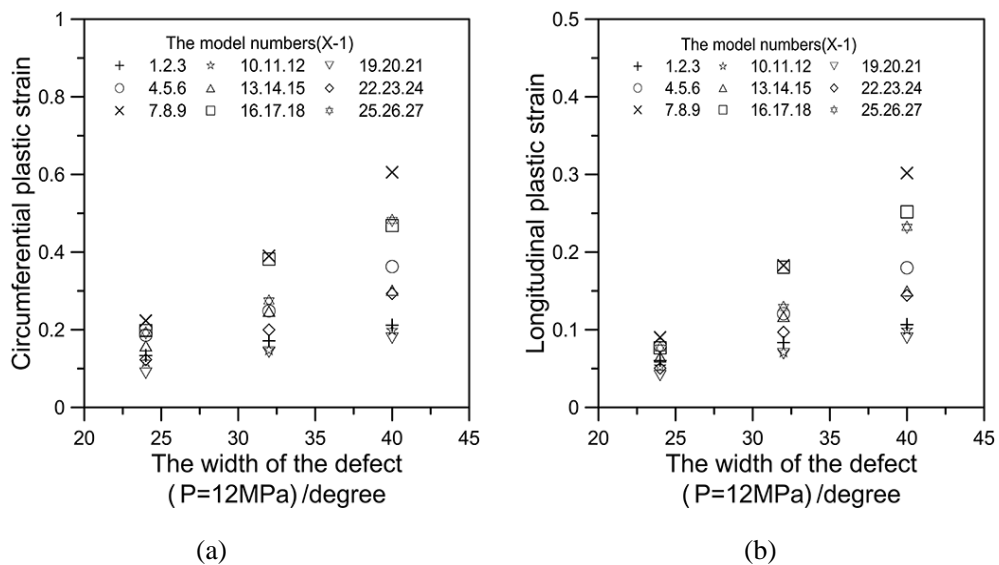
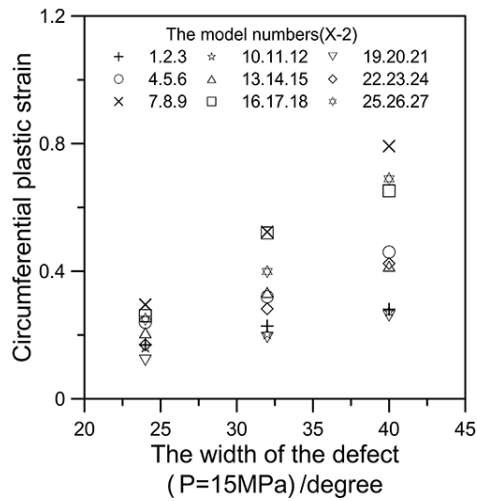


Fig. 9 Circumferential and longitudinal ratcheting strain versus number of cycles

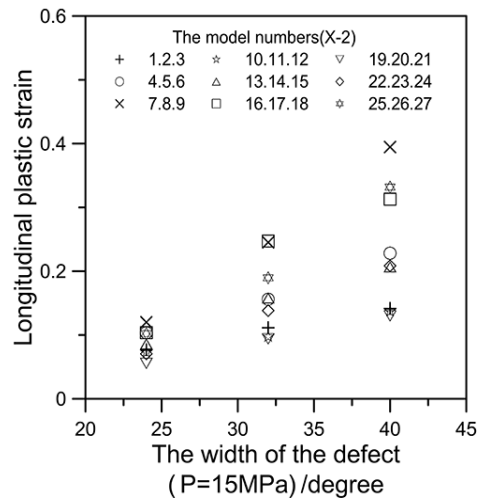
### 3.3.3 The effect of defect circumferential length on ratcheting strain

Ratcheting behavior of straight pipe subjected to internal pressure ( $P=12\text{MPa}$ ,  $15\text{MPa}$  and  $18\text{MPa}$ , respectively) and cyclic bending is affected by defect circumferential length, as given in Fig. 10. It indicates the relationship between hoop, axial ratcheting strain at position 1A and dimensionless defect circumferential length. Fig. 11 shows the relationship between ratcheting behavior and number of cycles. It is shown that the ratcheting strain increases with the increase of defect circumferential length.

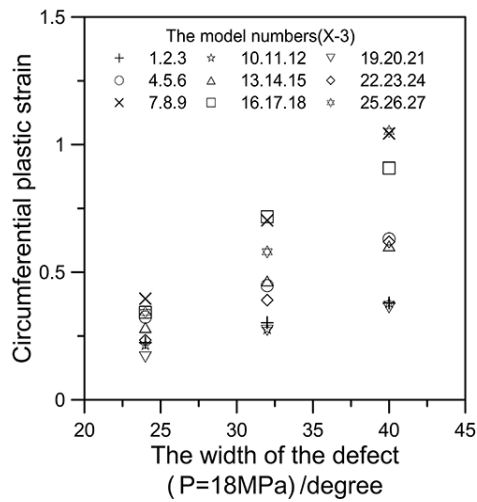




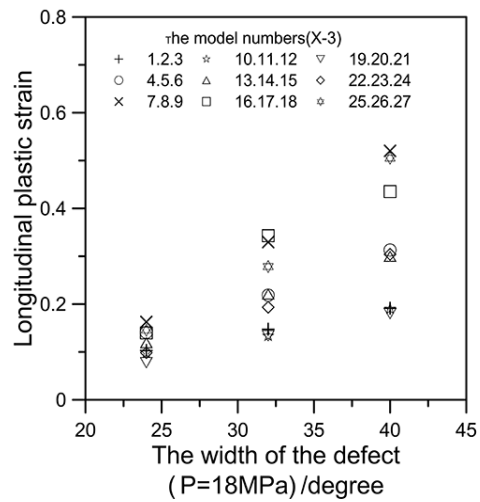
(c)



(d)

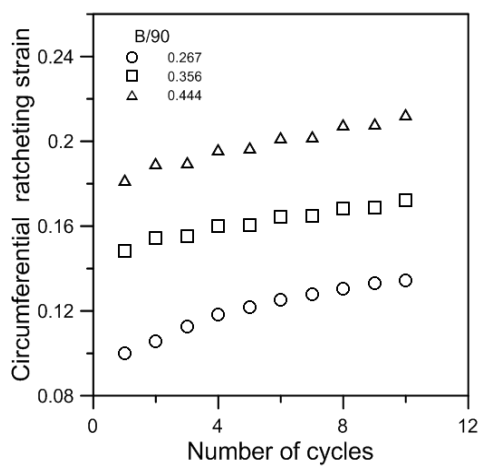


(e)

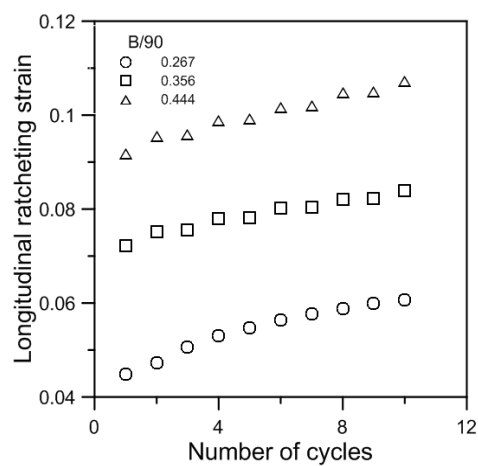


(f)

Fig. 10 Effect of defect circumferential length on ratcheting strain under different internal pressure



(a)

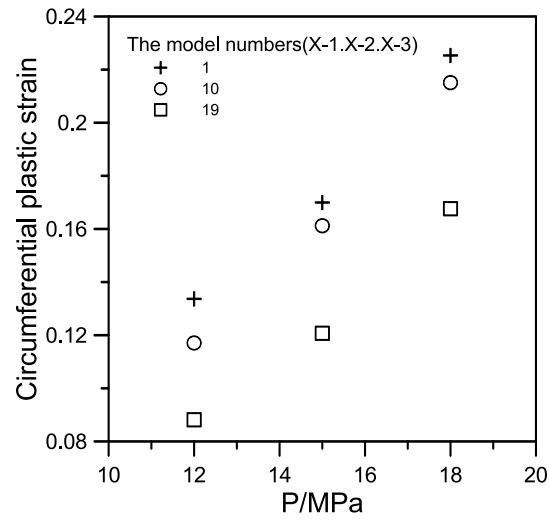


(b)

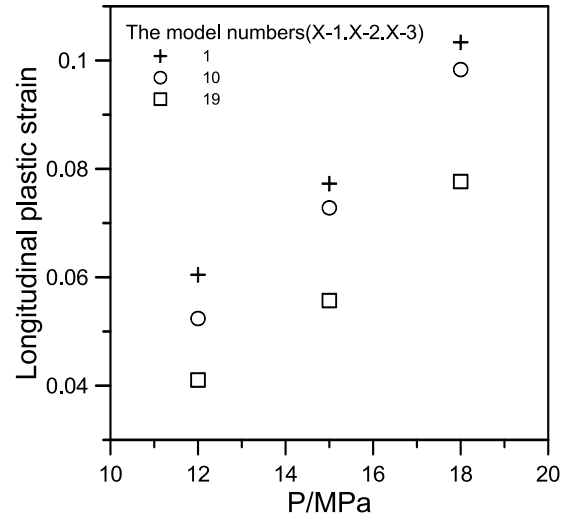
Fig. 11 Circumferential and longitudinal ratcheting strain versus number of cycles

### 3.3.4 The effect of internal pressure on ratcheting strain

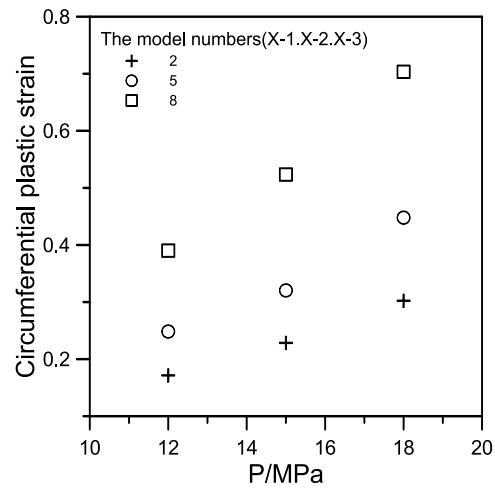
The effect of internal pressure ( $P=12\text{MPa}$ ,  $15\text{MPa}$  and  $18\text{MPa}$ , respectively) on ratcheting strain of straight pipe subjected to cyclic bending is shown in Fig. 12, where the hoop and axial ratcheting strain at position 1A is shown Fig. 13. It indicates that ratcheting strain increases with the increase of internal pressure.



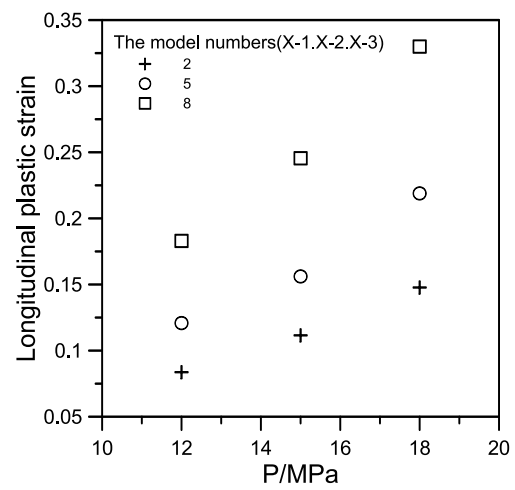
(a)



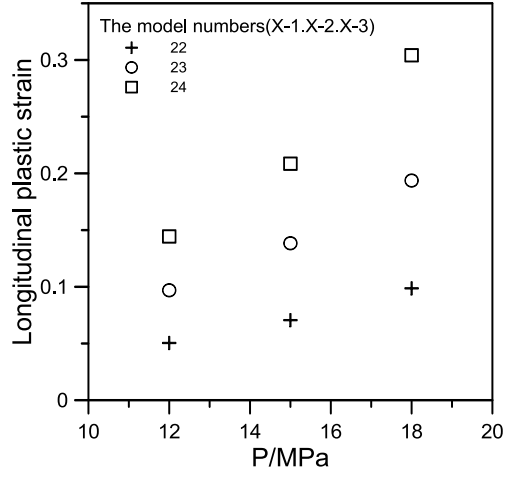
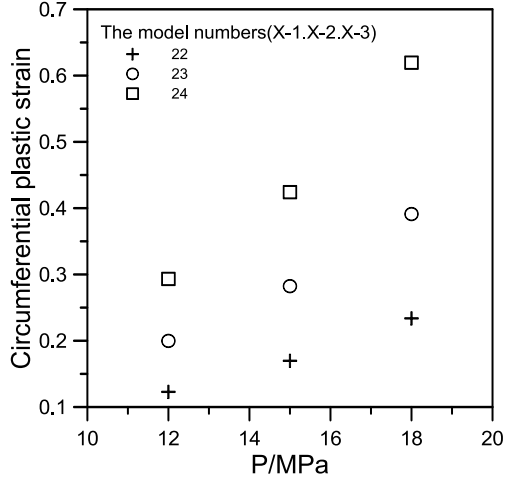
(b)



(c)



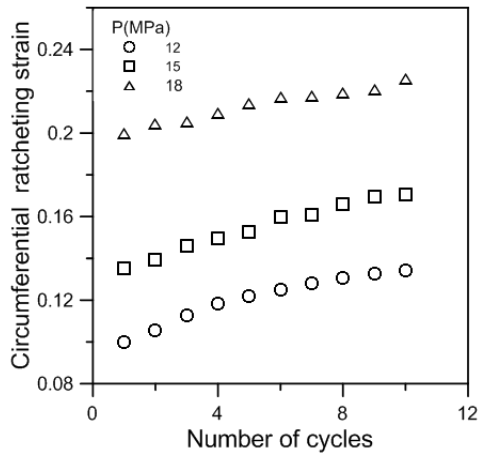
(d)



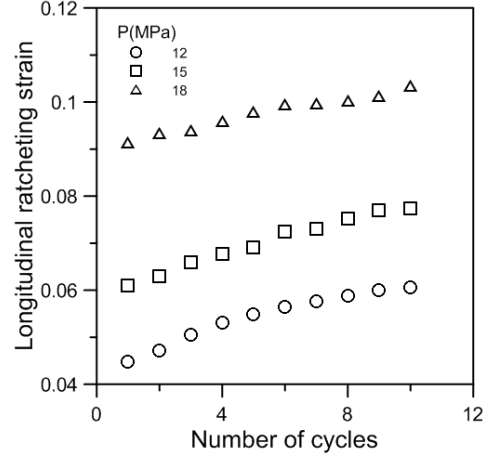
(e)

(f)

Fig. 12 The influence of internal pressure on ratcheting strain



(a)



(b)

Fig. 13 Circumferential and longitudinal ratcheting strain versus number of cycles

#### 4. Multiple regression method

In order to obtain the relationship between ratcheting strain of straight pipe and internal pressure, defect sizes, dimensionless relations are assumed as follows.

$$\varepsilon_{r\theta} = k_1 \left( \frac{P}{\sigma_{in}} \right)^{\alpha_1} \left( \frac{L}{D} \right)^{\alpha_2} \left( \frac{H}{T} \right)^{\alpha_3} \left( \frac{B}{90^\circ} \right)^{\alpha_4} \quad (9)$$

$$\varepsilon_{rz} = k_2 \left( \frac{P}{\sigma_{in}} \right)^{\beta_1} \left( \frac{L}{D} \right)^{\beta_2} \left( \frac{H}{T} \right)^{\beta_3} \left( \frac{B}{90^\circ} \right)^{\beta_4} \quad (10)$$

Taking the logarithm on both sides of Eq. (9) and (10), provides,

$$\ln(\varepsilon_{r\theta}) = \alpha_1 \ln\left(\frac{P}{\sigma_{in}}\right) + \alpha_2 \ln\left(\frac{L}{D}\right) + \alpha_3 \ln\left(\frac{H}{T}\right) + \alpha_4 \ln\left(\frac{B}{90^\circ}\right) + \ln k_1 \quad (11)$$

$$\ln(\varepsilon_{rz}) = \beta_1 \ln\left(\frac{P}{\sigma_{in}}\right) + \beta_2 \ln\left(\frac{L}{D}\right) + \beta_3 \ln\left(\frac{H}{T}\right) + \beta_4 \ln\left(\frac{B}{90^\circ}\right) + \ln k_2 \quad (12)$$

The parameters  $y_1$  and  $y_2$  represent  $\ln(\varepsilon_{r\theta})$  and  $\ln(\varepsilon_{rz})$ , respectively.  $\alpha_0$ , the parameters  $\beta_0$ ,  $x_1$ ,  $x_2$ ,  $x_3$  and  $x_4$  denote respectively  $\ln k_1$ ,  $\ln k_2$ ,  $\ln\left(\frac{P}{\sigma_{in}}\right)$ ,  $\ln\left(\frac{L}{D}\right)$ ,  $\ln\left(\frac{H}{T}\right)$  and  $\ln\left(\frac{B}{90^\circ}\right)$ . The general forms of multiple linear regression models are expressed by Eq. (13) and (14).

$$y_1 = \alpha_1 x_1 + \alpha_2 x_2 + \alpha_3 x_3 + \alpha_4 x_4 + \alpha_0 \quad (13)$$

$$y_2 = \beta_1 x_1 + \beta_2 x_2 + \beta_3 x_3 + \beta_4 x_4 + \beta_0 \quad (14)$$

where the parameters  $\alpha_{1-4}$  and  $\beta_{1-4}$  are regression coefficients, the parameters  $\alpha_0$  and  $\beta_0$  are random errors. The estimated values are expressed by the parameters  $b_{0-4}$ . Regression equation is written as follows:

$$\hat{y} = b_1 x_1 + b_2 x_2 + b_3 x_3 + b_4 x_4 + b_0 \quad (15)$$

Regression coefficients and random errors are estimated using the least square method, *i.e.*, when the sum of squared residuals the calculated value  $y$  and regression value  $\hat{y}$  reach the minimum, the estimated values are taken as the regression coefficients and random errors of regression equation.

According to the statistical analysis software (SPSS), the regression results are written in the following:

Hoop ratcheting strain:

$$\varepsilon_{r\theta} = 116.164 \left( \frac{P}{\sigma_{in}} \right)^{1.534} \left( \frac{L}{D} \right)^{-0.285} \left( \frac{H}{T} \right)^{2.368} \left( \frac{B}{90^\circ} \right)^{1.519} \quad (16)$$

Axial ratcheting strain:

$$\varepsilon_{rz} = 70.669 \left( \frac{P}{\sigma_{in}} \right)^{1.551} \left( \frac{L}{D} \right)^{-0.292} \left( \frac{H}{T} \right)^{2.203} \left( \frac{B}{90^\circ} \right)^{1.819} \quad (17)$$

The scopes of Eq.(16) and (17) are  $12\text{MPa} \leq P \leq 18\text{MPa}$  ,  $0.5 \leq L/D \leq 1$  ,  $0.5 \leq H/T \leq 0.7$  and  $24^\circ \leq B \leq 40^\circ$  .

The errors of finite element computed results and fitted values are calculated by Eq. (18) and (19).

Errors of hoop and axial ratcheting strain are listed in

Table 5.

$$e_{\theta} = \frac{\varepsilon_{r\theta} - \varepsilon_{n\theta}}{\varepsilon_{r\theta}} \times 100\% \quad (18)$$

$$e_z = \frac{\varepsilon_{rz} - \varepsilon_{nz}}{\varepsilon_{rz}} \times 100\% \quad (19)$$

It is shown in

Table 5 that the errors of finite element computed results and fitted values of most of models are within  $\pm 15\%$ . The regression results are acceptable.

Table 5 Error data

%

No.	$e_\theta$	$e_z$	No.	$e_\theta$	$e_z$	No.	$e_\theta$	$e_z$
1-1	19.466	20.974	10-1	16.464	17.345	19-1	-0.203	4.950
1-2	10.791	12.591	10-2	14.554	15.907	19-2	-3.048	0.971
1-3	10.987	13.275	10-3	15.275	17.372	19-3	1.801	5.752
2-1	2.953	3.737	11-1	-2.353	-2.684	20-1	3.905	4.854
2-2	-2.657	-2.117	11-2	-5.320	-5.950	20-2	-0.038	0.954
2-3	-2.642	-2.317	11-3	-1.725	-2.515	20-3	6.613	7.712
3-1	-10.268	-13.177	12-1	-6.851	-10.050	21-1	-7.583	-10.723
3-2	-17.119	-20.660	12-2	-9.345	-12.991	21-2	-3.993	-7.374
3-3	-14.743	-18.560	12-3	-4.320	-8.077	21-3	0.977	-2.817
4-1	11.087	10.800	13-1	5.379	0.658	22-1	-10.565	-15.315
4-2	2.806	2.578	13-2	-2.062	-6.174	22-2	-12.776	-16.601
4-3	4.885	5.037	13-3	1.213	-1.313	22-3	-8.368	-10.783
5-1	-3.234	0.345	14-1	6.044	7.000	23-1	-5.333	-1.398
5-2	-12.747	-9.048	14-2	1.752	2.483	23-2	-4.986	-0.437
5-3	-6.692	-3.210	14-3	6.893	7.469	23-3	-0.278	4.757
6-1	0.748	-0.461	15-1	-8.307	-9.144	24-1	-0.745	-2.203
6-2	-10.158	-11.884	15-2	-10.624	-11.893	24-2	1.885	-0.050
6-3	-6.292	-8.245	15-3	-0.932	-2.352	24-3	11.125	8.953
7-1	-6.739	-10.998	16-1	-9.639	-18.352	25-1	-1.865	-7.007
7-2	-13.776	-17.830	16-2	-16.914	-23.828	25-2	-10.406	-13.161

7-3	-12.158	-15.326	16-3	-17.604	-21.780	25-3	-6.406	-5.186
8-1	5.279	7.551	17-1	12.138	15.128	26-1	-10.587	-7.108
8-2	0.563	2.574	17-2	9.102	12.371	26-2	-6.999	-2.875
8-3	2.118	3.827	17-3	12.798	16.206	26-3	2.530	7.023
9-1	14.352	15.896	18-1	-0.584	8.666	27-1	11.677	10.667
9-2	7.758	9.085	18-2	-1.772	-3.930	27-2	13.103	11.690
9-3	7.428	8.483	18-3	3.315	0.876	27-3	24.590	23.036

## 5. Conclusions

In this study, the ratcheting behavior of pressurized corroded straight pipe under cyclic bending is investigated using Chaboche model. The effects of defect length, depth, width and internal pressure on ratcheting strain are researched. The obtained results indicate that ratcheting strain increases with the increase of defect length  $L/D$ , depth  $H/T$ , circumferential length and internal pressure. According to the orthogonal design method, an orthogonal table  $L_9(3^4)$  is established in order to analyze the ratcheting strain of corroded straight pipe. Dimensionless relations of both circumferential and longitudinal ratcheting strains to defect length, depth, width and internal pressure are established based on the multiple regression method. The scope of the dimensionless relation is  $12\text{MPa} \leq P \leq 18\text{MPa}$ ,  $0.5 \leq L/D \leq 1$ ,  $0.5 \leq H/T \leq 0.7$  and  $24^\circ \leq B \leq 40^\circ$ .

## Acknowledgments

This work was partly supported by the Natural Science Foundation of Hebei Province of China (No. E2018501022), Fundamental Research Funds for the Central Universities (No. N182304009), China Postdoctoral Science Foundation Funded Project (No: 2017M610171). The authors acknowledge

China Scholarship Council (CSC) which has supplied funding for us to undertake collaborative research.

## **References**

- [1] Prager W. A new method of analyzing stresses and strains in work hardening plastic solids. *J Appl Mech* 1956; 23: 493-496.
- [2] Besseling JF. A theory of elastic, plastic and creep deformations of an initially isotropic material. *J Appl Mech* 1958; 25: 529-536.
- [3] Armstrong P, Frederick C. A mathematical representation of the multiaxial bauchinger effect. CEGB Report No RD/BN 731, 1966.
- [4] Chaboche JL. Time independent constitutive theories for cyclic plasticity. *Int J Plast* 1986; 2: 149-188.
- [5] Chaboche JL. On some modifications of kinematic hardening to improve the description of ratcheting effects. *Int J Plast* 1991; 7: 661-678.
- [6] Chaboche JL. Modeling of ratcheting: evaluation of various approaches. *Eur J Mech A-Solid* 1994; 13: 501-518.
- [7] Bari S, Hassan T. An advancement in cyclic plasticity modeling for multiaxial ratcheting simulation. *Int J Plast* 2002; 18: 873-894.
- [8] Ohno N, Wang JD. Kinematic hardening rules with critical state of dynamic recovery, part I: formulations and basic features for ratcheting behavior. *Int J Plast* 1993; 9: 375-390.
- [9] Ohno N, Wang JD. Kinematic hardening rules with critical state of dynamic recovery, Part II: Application to Experiments of Ratcheting Behavior. *Int J Plast* 1993; 9: 391-403.

- [10] Chen X, Jiao R. Modified kinematic hardening rule for multiaxial ratcheting prediction. *Int J Plast* 2003; 20: 871–898.
- [11] Chen X, Jiao R, Kim KS. On the Ohno–Wang kinematic hardening rules for multiaxial ratcheting modeling of medium carbon steel. *Int J Plast* 2005; **21**: 161-84.
- [12] McDowell D. Stress state dependence of cyclic ratchetting behavior of two rail steels *Int J Plast* 1995; 11: 397-421.
- [13] McDowell D. An approximate algorithm for elastic-plastic two-dimensional rolling/sliding contact. *Wear* 1997; 211: 237-46.
- [14] Jiang YY, Sehitoglu H. Modeling of cyclic ratcheting plasticity, Part II: comparison of model simulations with experiments. *J Pres Ves - Trans ASME* 1996; 63: 726-733.
- [15] Jiang YY, Sehitoglu H. Modeling of cyclic ratcheting plasticity, Part I: development of constitutive relations. *J Pres Ves - Trans ASME* 1996; 63: 720-725.
- [16] Abdel-Karim M, Ohno N. Kinematic hardening model suitable for ratchetting with steady-state, *Int J Plast* 2000; 16: 225-240.
- [17] Halama R. A modification of abdelkarim-ohno model for ratcheting simulations. *Technical Gazette* 2008; 15: 3-9.
- [18] Rojíček J, Halama R. Numerical Simulations of Pipeline Bending Tests Applied and *Comput Mech* 2008; 2: 347-356.
- [19] Chen XH, Chen X, Yu DJ, Gao BJ. Recent progresses in experimental investigation and finite element analysis of ratcheting in pressurized piping. *Int J Pres Ves Pip* 2013; 101:113-142.
- [20] Varelis G E, Karamanos SA. Low-Cycle Fatigue of Pressurized Steel Elbows under In-Plane Bending. *J Pres Ves - Trans ASME* 2014; 137(1): 011401-1-10.

- [21] Varelis G E, Karamanos SA, Gresnigt AM. Pipe Elbows under Strong Cyclic Loading. *J Pres Ves - Trans ASME* 2013; 135(1), 011207-1-9.
- [22] Shi, H.R., Chen, G., Wang, Y. and Chen X. Ratcheting behavior of pressurized elbow pipe with local wall thinning. *Int J Pres Ves Pip* 2013; 102- 103:14-23.
- [23] Gudur S. Fatigue-ratcheting analysis of a pressurized elbow. *Int J Recent Adv Mech Eng* 2013; 2(3): 29-36.
- [24] Zakavi SJ, Ajri M, Golshan V. The ratcheting rate of stainless steel pressurized piping branch under seismic loading. *Indian J Sci Res* 2014; 3(1): 191-199.
- [25] Zakavi SJ, Ajri M, Golshan V. The ratcheting behaviour of plain carbon steel pressurized piping elbows subjected to simulated seismic in-plane bending. *World J Mech* 2014; 4: 238-246.
- [26] Zakavi SJ, Nourbakhsh M. The ratcheting behaviour of stainless steel pressurized piping elbows subjected to dynamic out-of-plane moments. *Mod Mech Eng* 2014; 4: 125-132.
- [27] Hassan T, Rahman M, Bari S. Low-cycle fatigue and ratcheting responses of elbow piping components. *J Pres Ves - Trans ASME* 2015; 137: 031010-1-12.
- [28] Hassan T, Rahman M. Constitutive models in simulating low-cycle fatigue and ratcheting responses of elbow. *J Pres Ves - Trans ASME* 2015; 137: 031002-1-12.
- [29] Wang L, Chen G, Zhu JB, Sun XH, Mei YH, Ling X, Chen X. Bending ratcheting behavior of pressurized straight Z2CND18.12N stainless steel pipe. *Struct Eng Mech* 2014; 52(6):1135-1156.
- [30] Chen XH, Chen X, Gang Chen, Duomin Li. Ratcheting behavior of pressurized Z2CND18.12N stainless steel pipe under different control modes. *Steel Compos Struct* 2015; 18(1): 29-50.
- [31] Fenton MA. Low-Cycle Fatigue Failure and Ratcheting Responses of Short and Long Radius Elbows at Room and High Temperatures. Master thesis, North Carolina State University, Raleigh,

North Carolina. 2015.

[32] Chen XH, Chen X, Weiwei Yu, Duomin Li. Ratcheting behavior of pressurized 90° elbow piping subjected to reversed in-plane bending with a combined hardening model. *Int J Pres Ves Pip* 2016; 137: 28-37.

[33] Chen XH, Chen X. Effect of Local Wall Thinning on Ratcheting Behavior of Pressurized 90° Elbow Pipe under Reversed Bending Using Finite Element Analysis. *Steel Compos Struct* 2016; 20(4): 931-950.

[34] Karamanos SA. Mechanical Behavior of Steel Pipe Bends; An Overview. *J Pres Ves - Trans ASME* 2016; 138(4): 041203.

[35] Chen XH, Chen X. Study on ratcheting effect of pressurized straight pipe with local wall thinning using finite element analysis. *Int J Pres Ves Pip* 2016, 139-140: 69-76

[36] Chen XH, Gao BJ, Chen X. Evaluation of AF type cyclic plasticity models in ratcheting simulation of elbow pipes under cyclic bending and steady internal pressure. *Steel Compos Struct* 2016, 21(4): 703-753

[37] Sabah M. Beden and Mohammed Kadhim Allawi. Fatigue Life Assessment of Petroleum Pipe Elbows. *Int J Current Eng Tech*, 2017, 7(1): 92-98.

[38] Hedayat A. S., Sloane N. J. A., and Stufken, J. *Orthogonal Arrays: Theory and Applications*, Springer, New York, NY, USA, 1999.

[39] Taguchi G., *Introduction to Quality Engineering: Designing Quality into Products and Process*, Asian Productivity Organization, Tokyo, Japan, 1986.

[40] Tan W, Lu YL, Dong JS. Structure Optimization of Rectangular Vessels Based on Limit Load Analysis. *Light Industry Machinery*, in Chinese, 2017, 35(4): 23-26.

[41] Sun YP, Wu XS, Dong JH, Yang LD, Gao BJ. Ratcheting boundary determination of pressurized lateral nozzle of cylinder subjected to cyclic in-plane bending. Pressure Vessel Technology, in Chinese, 2011, 28(7): 29-33.

[42] ABAQUS 6.13 Documentation

[43] ABAQUS 6.13 Example Problems Manual

[44] Cosham A, Hopkins P, Macdonald KA. Best practice for assessment of defects in pipeline-corrosion. Engineering Failure Analysis, 2007(14): 1245-1265.

[45] R5: An assessment procedure for the high temperature response of structures, Revision 2, British Energy, 2014.

[46] American Society of Mechanical Engineer. ANSI/ASME B31 G-1984 Manual for Determining the Remaining Strength of Corroded Pipelines. New York: ASME B31 Committee, 1984

[47] American Society of Mechanical Engineer. ANSI/ASME B31G-1991 Manual for Determining the Remaining Strength of Corroded Pipelines. New York: ASME B31 Committee, 1991.

[48] Chen G, Liu YH. Numerical theories and engineering methods for structural limit and shakedown analysis. Science Press, China, 2006.